nature communications

Article

https://doi.org/10.1038/s41467-026-75436-4

Temporal self-similarity reveals percolation universality classes in complex networks

Received: 13 April 2026

Accepted: 1 July 2026

Published online: 13 July 2026

Check for updates

Sheng Fang[1,12], Jun Meng[2,12], Qing Lin[1], Bingsheng Chen[3], Gaogao Dong[4], Chenglin Bai[5], Jan Nagler[6], Youjin Deng[7,8], Renaud Lambiotte[9] & Jingfang Fan[1,10,11]

Catastrophic fragmentation and structural transitions are ubiquitous in real-world complex systems, yet their underlying universality classes remain largely elusive due to strong structural heterogeneity and the absence of well-defined critical thresholds. Here, we discover a robust phenomenon of temporal self-similarity governing the dynamic percolation process across diverse complex networks. By tracking the full statistics of incremental growth events, we reveal that fragmentation dynamics are governed by two independent Fisher-type critical exponents, τ_c and τ_s. These exponents uniquely characterize the system's universality class, from which all other standard critical exponents can be derived through newly established scaling relations. After rigorously validating this framework on canonical network models, we apply it to extensive empirical datasets. Strikingly, our analyses across biological, social, and infrastructural systems demonstrate that real-world networks systematically exhibit universality classes distinct from those predicted by idealized network models, reflecting the influence of higher-order structural features. Our findings establish a dynamic paradigm that bridges statistical physics and real-world resilience, offering a parameter-free, highly scalable approach to classify and characterize structural vulnerabilities in inherently heterogeneous systems.

Understanding how large-scale connectivity is lost in heterogeneous systems is a central challenge across network science, statistical physics, biology, and infrastructure research[1–8]. In these diverse settings, a key concept is resilience: the ability of a system to maintain global connectivity and functionality under external perturbations[9–13]. Percolation theory provides a fundamental and widely adopted framework to model such connectivity transitions, predicting that near a critical threshold, systems exhibit abrupt macroscopic breakdowns and scale-invariant behaviors[7,14–20]. As shown in Fig. 1, progressive removal of bonds or nodes can trigger the breakdown of a giant connected component with a critical threshold q_c. Near q_c, the size of the largest connected component follows characteristic scaling laws governed by critical exponents such as β. While different networks may exhibit distinct values of q_c and β depending on their topological

[1]School of Systems Science, Beijing Normal University, Beijing, China. [2]State Key Laboratory of Earth System Numerical Modeling and Application, Institute of Atmospheric Physics, Chinese Academy of Sciences, Beijing, China. [3]Network Science Institute and Department of Physics, Northeastern University, Boston, MA, USA. [4]School of Mathematical Sciences, Jiangsu University, Zhenjiang, Jiangsu, China. [5]School of Mathematics and Systems Science, Liaocheng University, Liaocheng, Shandong, China. [6]Deep Dynamics, Centre for Human and Machine Intelligence, Frankfurt School of Finance and Management, Frankfurt am Main, Germany. [7]Department of Modern Physics, University of Science and Technology of China, Hefei, Anhui, China. [8]Hefei National Laboratory, University of Science and Technology of China, Hefei, China. [9]Mathematical Institute, University of Oxford, Oxford, UK. [10]Potsdam Institute for Climate Impact Research, Potsdam, Germany. [11]State Key Laboratory of Marine Environmental Science, Xiamen University, Xiamen, China. [12]These authors contributed equally: Sheng Fang, Jun Meng. e-mail: jingfang@bnu.edu.cn

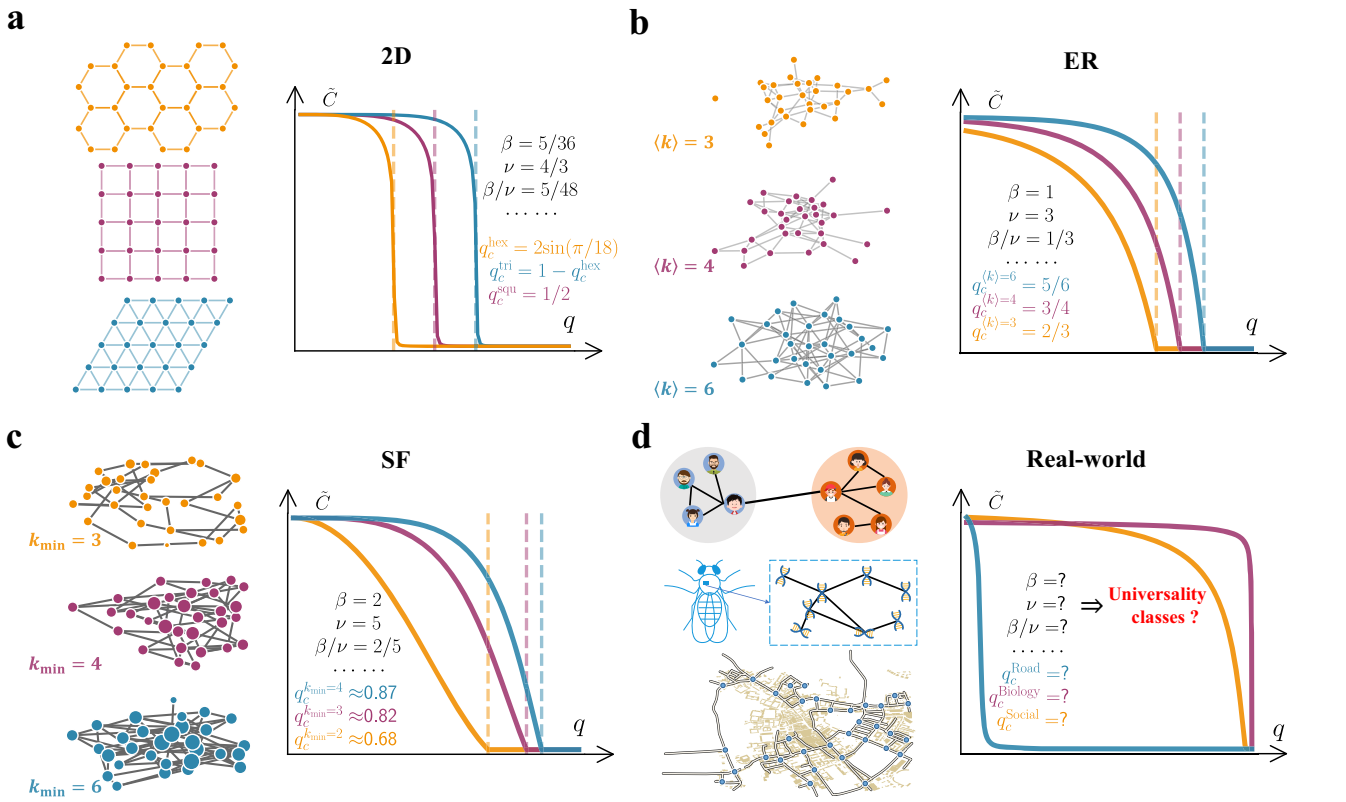


Fig. 1 | Illustration of network topology and resilience across model-generated and real-world systems. Resilience is characterized by the rescaled size of the largest connected component, $\tilde{C} = C/V$ with the largest cluster C and system volume V, as a function of the bond removal fraction q. Subfigures (**a**–**c**) present representative model networks: (**a**) two-dimensional lattices (regular), **b** Erdős--Rényi networks (random), and (**c**) scale-free networks (heterogeneous). For such model systems, critical thresholds and exponents can be derived analytically, and universal features such as critical exponents are independent of microscopic network details. Subfigure (**d**) shows real-world networks from social, biological, and road categories. In these systems, both critical thresholds and critical exponents are generally non-universal and must be determined empirically.

structure, percolation theory predicts that systems differing in microscopic details can nonetheless display identical scaling behavior, a hallmark of universality.

While traditional percolation theory has yielded elegant universal scaling laws for idealized model systems[8,21,22], extracting such universal behavior from real-world networks remains highly problematic[23]. As illustrated in Fig. 1(a)-(c), for canonical systems such as two-dimensional lattices (2D), Erdös-Rényi (ER) networks, and scale-free (SF) networks, the critical thresholds and exponents of bond percolation can be obtained through analytical approaches or numerical finite-size scaling (FSS) analysis. Despite differences in lattice geometry, dimensionality, or degree distribution, such systems exhibit robust universal behavior near criticality, characterized by several exponents, such as the order-parameter exponent β and correlation-length exponent ν[24–26]. However, empirical systems are inherently finite, strongly heterogeneous, and lack well-defined spatial locality. Moreover, recent studies reveal that percolation in empirical systems is often heavily modulated by feature-enriched interactions, adaptive local feedback, and higher-order coupling patterns[27–31]. In parallel, recent work on cascading dynamics has revealed that complex systems can exhibit hybrid or system-specific universality classes beyond classical expectations[32]. These structural and dynamic complexities completely obscure the true critical thresholds, rendering standard static FSS procedures ineffective for extracting critical exponents, as shown in Fig. 1d. Consequently, a crucial question remains unanswered: what universality classes actually govern the catastrophic collapse of highly heterogeneous, real-world complex systems?

To overcome these fundamental limitations, we propose an event-based gap-statistics framework that characterizes percolation through the ordered sequence of bond-addition events. The gap-based perspective was introduced to study the largest jump of the largest connected component during the percolation process[33]. In that framework, the largest gap was treated as a single extreme-event observable: its location identifies a pseudocritical threshold, while the finite-size scaling of its magnitude, location, and associated cluster size provides information about the critical behavior of the transition. Building on this foundation, the present work moves beyond the largest-gap observable by generalizing the analysis to the full statistical distribution of growth gaps, $n(G, V, r)$, accumulated along the percolation trajectory. This distribution-level formulation reveals a robust form of temporal self-similarity in both the critical and supercritical regimes. Specifically, the gap-size distribution exhibits persistent power-law scaling governed by two independently measurable Fisher-type gap exponents, τ_c and τ_s, characterizing the critical and supercritical regimes, respectively. Through the scaling relations derived below, these exponents provide a compact gap-based parametrization of percolation universality classes and allow other standard critical exponents to be inferred within the framework of renormalization-group scaling theory[34–38]. This approach bypasses the need for exact critical thresholds or multiple system sizes, making it particularly useful for empirical networks. Here, the terms “dynamic” and

"temporal" refer to the ordered sequence of bond-addition events in the percolation growth process, rather than to an autonomous physical time evolution.

Strikingly, by applying this dynamic theoretical framework to extensive empirical datasets, we reveal that real-world networks exhibit profound deviations from classical theories. Although many empirical networks feature heterogeneous degree distributions resembling SF networks, their measured critical exponents (τ_c, τ_s) significantly diverge from the predictions of idealized SF models. This result indicates that real-world networks cluster into distinct universality classes that are not captured by idealized SF models. The specific values of these dynamic exponents reflect how structural correlations and community structure can substantially limit cascading failures or accelerate systemic collapse, offering a direct physical interpretation of resilience in heterogeneous topologies.

Our results demonstrate that the dynamic gap-size distribution captures universal features of fragmentation processes across a wide range of complex systems. Importantly, the proposed method enables the extraction of universality classes without requiring prior knowledge of critical thresholds or access to multiple system sizes. By unifying theoretical analysis, extensive numerical validation, and application to real-world biological, social, and infrastructural networks, our work establishes a scalable and physically interpretable framework for probing universality, resilience, and structural transitions in heterogeneous complex systems.

Results

Universal scaling behaviors of gaps

We begin by examining the statistical properties of growth gaps that emerge during the percolation process. Specifically, we analyze both the mean $\bar{(\cdot)}$ and the fluctuation $\chi_{(\cdot)}$ of several key quantities associated with the largest connected component, namely the gap location r_m, the gap magnitude Δ_m, and the size of the largest cluster evaluated at the gap location, $C_m = C(r_m)$. Here, the subscript m denotes the order of the gap, with m = 1 corresponding to the largest gap, as defined in Methods.

For m = 1, these quantities follow well-defined FSS relations, as previously established in Ref. 33:

$$\begin{aligned} \bar{\Delta}_1(V) &\sim V^{-\beta_1},\ \chi_{\Delta_1}(V) \sim V^{-\beta_2}, \\ |\bar{r}_1(V) - r_c| &\sim V^{-1/\nu_1},\ \chi_{r_1}(V) \sim V^{-1/\nu_2}, \\ \bar{C}_1(V) &\sim V^{d_{f_1}},\ \chi_{C_1}(V) \sim V^{d_{f_2}}, \end{aligned} \tag{1}$$

where r_c denotes the critical threshold in the thermodynamic limit $V \to \infty$. Typically, one usually has $\nu_1 = \nu_2 = \nu$, where ν is the conventional correlation-length exponent. However, this equality does not always hold. In particular, cases with $\nu_1 \neq \nu_2$ have been reported in some percolation models[33,39–41]. Therefore, we keep ν_1 and ν_2 distinct in the general scaling formulation. In addition, $\beta_1 = \beta_2 = \beta/\nu$ represent the order-parameter exponent rescaled by ν, and $d_{f_1} = d_{f_2} = d_f$ denote the fractal dimension of the critical cluster. Throughout this work, FSS behavior is expressed in terms of the system volume V, defined as the number of nodes or sites, rather than the linear size L. This convention is adopted because many networks, especially empirical networks, do not possess a well-defined Euclidean dimension or linear size.

To assess whether these scaling properties extend beyond the largest gap, we analyze the top five gaps of the largest cluster for bond percolation on the 2D square lattice. Figure 2 shows the dependence of these quantities on the system volume V on a log-log scale. Remarkably, the mean values and fluctuations associated with different gap orders collapse onto lines with identical slopes, indicating that all top gaps obey the same scaling behavior.

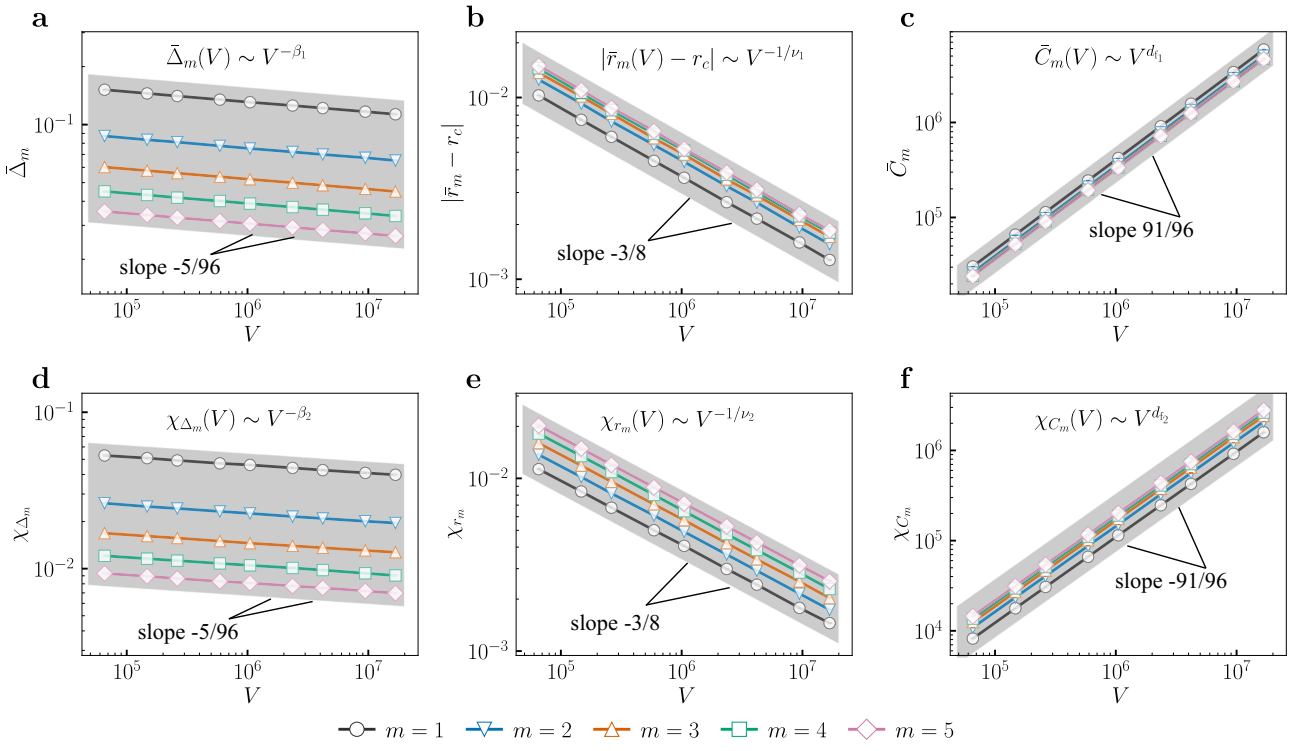


Fig. 2 | Universal scaling behaviors of the top five gaps in bond percolation on the square lattice with volume *V*. Panels (**a**–**c**) display the average values of the gap $\bar{\Delta}_m$, the deviation of the pseudo-critical point from the critical threshold $|\bar{r}_m - r_c|$, and the size of the largest cluster corresponding to each gap C_m, respectively. Panels (**d**–**f**) illustrate the corresponding fluctuations. Error bars are smaller than the symbol sizes in all panels. These results indicate consistent scaling behavior for both averages and fluctuations across the top five gaps. The shaded regions serve as a visual guide to highlight the consistent slopes across the five gap orders.

We further perform least-squares fitting to the Monte Carlo simulation data, and the resulting estimates of the scaling exponents are summarized in Supplementary Table 1. The fitted values confirm that the scaling exponents are independent of the gap order m, revealing a robust form of universality across multiple gap events. Importantly, this behavior is not restricted to 2D lattices. As shown in Supplementary Fig. 1, analogous scaling relations are observed for bond percolation on ER networks, where the mean values and fluctuations of the top five gaps again follow identical power-law dependencies on system size.

Temporal self-similarity

The numerical results above demonstrate that the top five gaps associated with the growth of the largest connected component exhibit identical scaling behavior. This observation naturally raises a fundamental question: how many gap events follow the same scaling laws, and whether such regularity reflects a deeper form of self-similarity in the percolation dynamics.

To motivate this idea, we first recall a well-established result from FSS theory. Near criticality, the number density of clusters of size s obeys[20,26],

$$n(s,V) = n_0 s^{-\tau}\tilde{n}(s/V^{d_f}), \tag{2}$$

where n_0 is a nonuniversal amplitude and τ is the Fisher exponent. The exponent τ is related to the fractal dimension d_f through the hyperscaling relation,

$$\tau = 1 + 1/d_f. \tag{3}$$

As a consequence, the number of clusters with size of order $O(V^{d_f})$,

$$N_s = V\sum\nolimits_{s=O(V^{d_f})} n(s,V), \tag{4}$$

remains finite in the thermodynamic limit. This result implies that, for any finite m, the top m largest clusters exhibit identical scaling behavior, reflecting a form of spatial self-similarity at criticality. This case is very similar to our observation above that the unnormalized top-m (m = 5) gap values have the same scaling behavior $V\bar{\Delta}_m \sim V^{d_f}$ with $d_f = 1-\beta/\nu = 1-\beta_1$. In contrast to the common static viewpoint, the gap events considered here arise from the temporal evolution of the dynamic percolation process. This distinction motivates the central hypothesis of our work: if spatial self-similarity governs the statistics of large clusters at criticality, then an analogous form of self-similarity may emerge in time through the sequence of growth gaps experienced by the largest connected component. We refer to this dynamic counterpart along the event-based percolation trajectory as temporal self-similarity.

Guided by this intuition, we hypothesize that the scaling behavior observed for the top five gaps can be generalized to the top m gaps for any finite m. To test it, we introduce the gap-size distribution $n(G, V, r)$, defined at bond fraction r as the cumulative distribution of all gap events of magnitude G occurring during the percolation process from r = 0 up to r. This construction parallels the cluster-size distribution $n(s, V)$, but characterizes the statistics of dynamic growth events rather than static cluster configurations.

Figure 3a shows the evolution of the rescaled largest cluster $\tilde{C} = C/V$ for bond percolation on the two-dimensional square lattice, while Figs. 3b–d illustrate representative configurations in the subcritical, critical, and supercritical regimes, respectively. In the subcritical phase, clusters remain small, and both the magnitude and frequency of growth events of the largest cluster are limited, resulting in a small value of $n(G, V, r)$. As the system approaches the critical threshold, large merging events become increasingly frequent, leading to a rapid increase in the gap-size distribution.

The corresponding scaling behavior of $n(G, V, r)$ across different regimes is shown in Supplementary Fig. 2. We find that the gap-size distribution exhibits a clear power-law scaling behavior at criticality and persists into the supercritical phase. Moreover, since the location of the largest gap r_1 follows the same FSS behavior as the thermodynamic critical threshold r_c, we expect the scaling properties of $n(G, V, r)$ evaluated at $r = r_1$ and at $r = r_c$ to be identical in the large-system limit.

We then investigate $n(G, V, r)$ at r_1 and at full bond occupation $r_E = E/V$, where E is the total number of bonds. The corresponding results for bond percolation on the two-dimensional square lattice are shown in Fig. 3e, i. In the log-log scale, the gap-size distributions initially follow a power-law scaling with two distinct exponents τ_c and τ_s, and decay rapidly when the gap size G exceeds a characteristic cut-off. The cut-off scale grows with system size as $O(V^{d_f})$, consistent with the scaling of the largest gap, $V\bar{\Delta}_m \sim V^{d_f}$, as shown in Fig. 2. At $r = r_1$, the exponent τ_c is measured to be ~1.60, which differs significantly from the Fisher exponent of two-dimensional percolation, $\tau = 187/91$. This deviation signals a breakdown of the standard hyperscaling relation in Eq. (3). Moreover, we find that the amplitude of $n(G, V, r_1)$ exhibits explicit dependence on the system size V, rather than remaining constant as in the conventional cluster-size distribution. Motivated by these observations, we propose the generalized scaling form[42],

$$n(G,V,r) = n_0 V^{-\kappa} G^{-\tau_c}\tilde{n}(G/V^{d_f}), \tag{5}$$

which reduces to the standard cluster-size scaling form in Eq. (2) when $\kappa = 0$.

We now examine the origin and values of the exponents κ and τ_c. Our central assumption is that large gap events are dominated by contributions arising within the critical window, whose width scales as $O(V^{-1/\nu_1})$. This assumption can be justified by comparing contributions from different regimes of the percolation process. When the system is far from criticality, $t = r_c - r = O(1)$, the largest cluster remains small, and its growth increments are bounded by O (ln V). In this regime, the probability that a newly added bond contributes to the growth of the largest cluster scales as $1/V$, implying a negligible contribution. As the bond occupation approaches criticality according to $t \sim V^{-\lambda}$ with $\lambda < 1/\nu_1$, the largest cluster grows as $V^{\lambda\nu_1 d_f}$. Consequently, the gap-size density scales as,

$$n(G,V) \sim V^{-\lambda+\lambda\nu_1 d_f - 1} = V^{-(\lambda+1-\lambda\nu_1 d_f)}. \tag{6}$$

For all $\lambda < 1/\nu_1$, the exponent $(\lambda + 1 - \lambda\nu_1 d_f)$ exceeds κ, indicating that contributions from outside the critical window are subdominant.

Within the critical window, the scaling parameter satisfies $\lambda = 1/\nu_1$. In this regime, the gap-size distribution follows,

$$n(G,V,r_1) \sim V^{-1/\nu_1 + d_f - 1}, \tag{7}$$

which yields,

$$\kappa = \frac{1}{\nu_1} + 1 - d_f. \tag{8}$$

Based on this result, the requirement that the number of gaps of order $O(V^{d_f})$ remains finite leads to a modified hyperscaling relation,

$$\tau_c = 1 + \frac{1-\kappa}{d_f} = 2 - \frac{1}{\nu_1 d_f} = 2 - \sigma, \tag{9}$$

where $\sigma = (\nu_1 d_f)^{-1}$ is the critical exponent governing the divergence of the characteristic cluster size in the cluster-number density $n(s)$.

https://doi.org/10.1038/s41467-026-75436-4

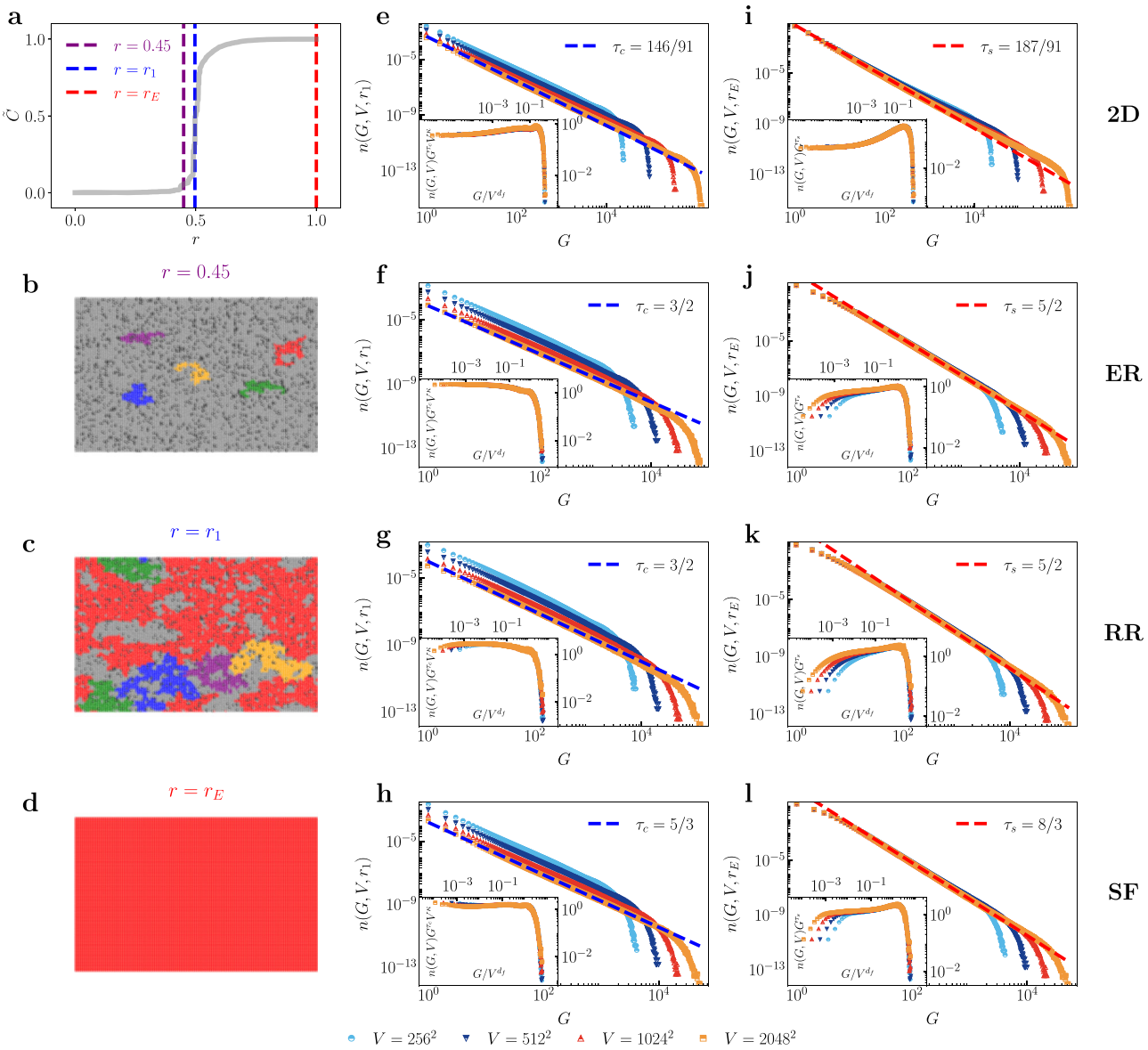


Fig. 3 | Temporal self-similarity of the gap-size distribution $n(G, V, r)$ in critical and supercritical regimes. a Evolution of the rescaled largest cluster $\bar{C}$ as a function of bond occupation probability r for bond percolation on a square lattice of volume $V = 128^2$. Vertical dashed lines indicate three regimes: subcritical ($r = 0.45$), critical ($r = r_1$), and supercritical ($r = r_E$). **b**–**d** Representative configurations at each regime, with the largest cluster shown in red. **e**–**h** Critical gap-size distribution $n(G, V, r_1)$ versus gap size G in log--log scale for four network models: two-dimensional lattice (2D), Erdős-Rényi (ER), random regular (RR), and scale-free (SF, $\gamma = 3.5$). **i**–**l** Corresponding distributions $n(G, V, r_E)$ in the supercritical regime. Insets in (**e**–**l**) show data collapses of $n(G, V, r)$ guided by Eq. (5). The good collapse in each panel supports the conjectured scaling relations given in Eqs. (5), (3), and (9).

For 2D percolation, this relation predicts $\tau_c = 2 - \sigma = 146/91 = 1.604\ldots$, in excellent agreement with the numerical measurements. To further refine the estimate of τ_c, we compute the total number of gaps, $N_G = V\sum_G n(G, V)$ at $r = r_1$, which is expected to scale as $N_G \sim V^{1-\kappa}$ according to Eq. (5).

Our numerical results indeed yield $N_G \sim V^{1-\kappa}$ with $\kappa = 0.41(1)$, corresponding to $\tau_c = 1.62(1)$. As shown in the inset of Fig. 3e, rescaling $n(G, V, r)V^{\kappa}G^{\tau_c}$ against G/V^{d_f} produces an excellent data collapse, providing strong support for the proposed scaling form. In contrast, at full bond occupation $r = r_E = E/V$ (Fig. 3i), the gap-size distribution is characterized by a power-law exponent $\tau_s \approx 2.05$, while the amplitude n_0 becomes independent of the system size, implying $\kappa = 0$. In this limit, the modified hyperscaling relation in Eq. (9) reduces to the conventional hyperscaling relation in Eq. (3). As a result, the exponent τ_s, which characterizes temporal gap statistics in the supercritical regime, coincides with the Fisher exponent τ describing spatial self-similarity of critical clusters. This correspondence is further confirmed by the second moment of the gap-size distribution, $S_2 = \sum_G G^2 n(G, V)$, which is expected to scale as $S_2 \sim V^{d_f(3-\tau_s)}$.

We next extend the analysis to other model-generated networks, including ER, random regular (RR), and SF networks with degree exponent $\gamma = 3.5$, and results for other γ values are shown in Supplementary Fig. 4. Theoretical prediction of percolation critical exponents on SF networks is presented in the Method. Compared with the 2D lattice, ER and RR networks introduce increasing levels of structural randomness, while SF networks further incorporate strong topological heterogeneity through broad degree distributions. Following the same analytical procedure, we observe qualitatively identical scaling behavior of the gap-size distribution across all network classes, as shown in Fig. 3. The plots of N_G and S_2 are presented in Supplementary Fig. 3,

Table 1 | The critical exponents τ_c and τ_s of the gap-size distribution at criticality and supercriticality

	κ	τ_c	d_f	τ_s
2D	0.41(1)	1.62(1)	0.947 9(2)	2.055(1)
	41/91	146/91	91/96	187/91
ER	0.668(2)	1.498(4)	0.666(4)	2.499(5)
	2/3	3/2	2/3	5/2
RR	0.667(2)	1.500(3)	0.666(2)	2.499(5)
	2/3	3/2	2/3	5/2
SF	0.600(2)	1.664(4)	0.602(2)	2.661(6)
	3/5	5/3	3/5	8/3

For each network, the first row is the estimate from numerical simulation, and the second row is the theoretical prediction. The Fisher exponents τ_c and τ_s are derived from the FSS analysis of N_G and S_2, respectively, and other exponents can be derived from the hyperscaling relations Eq. (3) and Eq. (9).

and the corresponding estimates of the critical exponents are summarized in Table 1. Remarkably, despite substantial differences in microscopic topology, the exponent τ_s consistently coincides with the standard Fisher exponent τ of the corresponding percolation universality class. This agreement demonstrates that the supercritical gap statistics preserve classical universality across diverse network models. In contrast to the typical method, which requires both the exact value of the critical threshold and the cluster number density to extract the Fisher exponent, our approach can directly determine the exponent τ_s in any supercritical regime using only the gap-size distribution.

An important advantage of the dynamic gap-scaling framework is that it enables the extraction of two independent critical exponents, τ_c and τ_s, without requiring precise knowledge of the percolation threshold. In particular, the exponent τ_s can be robustly obtained solely from the supercritical regime, where the largest connected component is already established. This feature is especially relevant for real-world systems, in which the critical point is often inaccessible or ill-defined. Here, the two Fisher-type exponents τ_c and τ_s should be understood as two independently measurable gap-based descriptors, rather than as new fundamental exponents outside standard scaling theory. They are obtained from two distinct regimes of the gap-size distribution: τ_c characterizes the critical regime near $r = r_1$, whereas τ_s characterizes the supercritical regime at $r = r_E$. Through the scaling relations derived below, these exponents provide a compact gap-based parametrization of conventional critical behavior and offer a practical route for inferring universality classes from gap statistics.

To elucidate the physical origin of the two distinct exponents, we consider the dynamical evolution of gap formation throughout the percolation process. As the bond occupation probability increases, the largest connected component grows through a sequence of merging events whose statistics depend strongly on the proximity to criticality. In the subcritical phase ($r < r_c$), clusters remain small and disconnected. Both the size of the largest cluster and the magnitude of its growth increments are bounded by $O(\ln V)$, leading to a limited number of significant gap events, with $N_G \sim O(1)$. At this stage, the probability that a newly added bond contributes to the growth of the largest cluster scales as $1/V$, so only a few bond additions produce noticeable changes in C. As the system approaches the critical point, entering the critical regime, both the size of the largest cluster C and the typical gap magnitude G increase sharply from $O(\ln V)$ to $O(V^{d_f})$. This rapid growth is accompanied by a dramatic increase in the number of gap events, with N_G rising from $O(1)$ to $O(V^{1-\kappa})$. In this regime, bond additions are increasingly likely to trigger macroscopic merging events, reflecting the emergence of long-range correlations and the onset of critical behavior. In the supercritical phase ($r > r_c$), the largest connected component spans the entire system and occupies a finite fraction of all nodes. As a consequence, nearly every newly added bond contributes to its growth, leading to $N_G \sim O(V)$. However, the incremental increase in cluster size becomes progressively smaller, preventing further growth of the cut-off scale in the gap-size distribution. As a result, the system enters a saturated regime in which gap formation remains frequent but no longer generates large fluctuations.

These dynamical regimes are directly reflected in the numerical gap-size distributions shown in Supplementary Fig. 2, which clearly distinguish subcritical, critical, and supercritical behavior. Taken together, the sharp increase of both the largest cluster size and the number of gap events near criticality, followed by saturation in the supercritical phase, encodes the intrinsic dynamics of the percolation transition. This structure naturally gives rise to two independent scaling exponents, enabling a dynamic characterization of universality beyond traditional static approaches.

Percolation on real-world networks

A central advantage of the gap-size distribution is its ability to characterize critical phenomena in percolation and related complex systems through dynamic statistics rather than static configurations. The two Fisher-type exponents, τ_c and τ_s, are independent and together form a complete set of critical descriptors, from which other standard critical exponents can be derived through scaling relations rooted in RG theory. Importantly, the estimation of τ_c and τ_s does not require prior knowledge of the critical threshold r_c and is independent of system size, thereby circumventing the limitations of traditional FSS approaches. This feature makes the method particularly suitable for real-world networks, where only a single system realization is typically available.

We apply the framework to bond percolation on a diverse set of real-world networks and analyze the gap-size distribution $n(G, V, r)$ evaluated at the location of the largest gap r_1 and at full bond occupation $r = r_E$. Compared with model-generated networks, real systems exhibit far greater structural complexity and heterogeneity. As illustrated in Fig. 1, different real-world networks possess markedly distinct topological characteristics. For example, social networks often contain highly connected hubs, resembling SF structures, whereas road networks display narrow degree distributions constrained by spatial embedding, similar to planar lattices. Recent studies on modular interacting infrastructures and multimodal transport systems further show that interconnected design can either mitigate or amplify critical fragmentation, depending on coupling architecture and flow constraints[4,11].

Using the network datasets compiled in Ref. 43, we perform percolation simulations on networks drawn from a broad range of domains, including biological, citation, coauthor, interaction, recommendation, social, scientific computing, road, and gene networks. Detailed structural information for each system is summarized in Supplementary Table 2. Figures 4a–i show the resulting gap-size distributions $n(G, V)$ as functions of gap size G for both $r = r_1$ and $r = r_E$ on a log-log scale.

Despite their strong structural differences, all real-world networks exhibit gap-size distributions with clear power-law regimes, analogous to those observed in model-generated systems. The distributions follow different scaling exponents across networks, reflecting intrinsic structural diversity. Because large gap events are concentrated near criticality, the distributions evaluated at $r = r_1$ and $r = r_E$ collapse onto each other in the large-G regime. Reference power-law lines, shown as red and blue dashed lines in each panel, illustrate the scaling behavior and demonstrate excellent agreement with the numerical data. To quantify these observations, we perform least-squares fitting of the data of $n(G, V, r)$ to extract the critical exponents τ_c and τ_s (see "Method" for details), with the results summarized in Table 2. Across all real-world networks considered, the exponents satisfy the bounds $\tau_s \in [2, 3)$ and $\tau_c \in (1, 2]$, consistent with theoretical constraints. Each network is therefore characterized by a distinct pair (τ_c, τ_s), which serves as a compact descriptor of its fragmentation dynamics.

https://doi.org/10.1038/s41467-026-75436-4

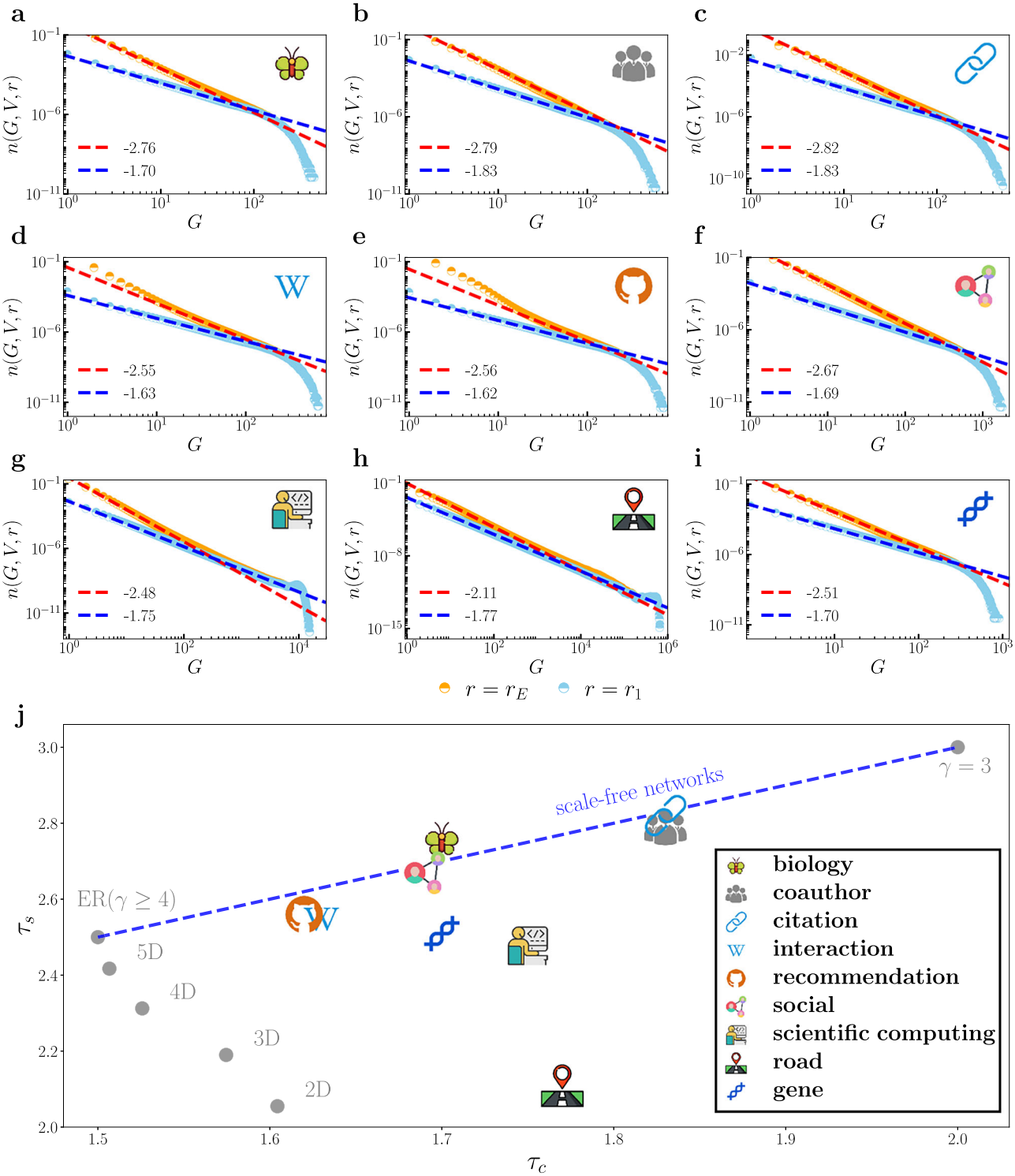


Fig. 4 | Universality classes of percolation on real-world networks characterized by a pair of independent critical exponents (τ_c, τ_s). a–i Gap-size distribution $n(G, V)$ versus gap size G plotted on log-log scale for nine real-world networks: (a) biology, (b) coauthor, (**c**) citation, (**d**) interaction, (**e**) recommendation, (**f**) social, (**g**) scientific computing, (h) road, and (i) gene networks. The detailed information of these real-world networks is shown in Supplementary Table S2. In each panel, the power-law exponents of $n(G, V, r)$ at r_1 and r_E are denoted as τ_c and τ_s, respectively. **j** Relation between τ_c and τ_s across different networks. The gray dashed line indicates the universality class for scale-free networks with $\gamma \geq 3$. The obtained Fisher exponents τ_c and τ_s for all real-world networks are summarized in Table 2.

Through the hyperscaling relations in Eqs. (3) and (9), the fractal dimension d_f and correlation-length exponent ν_1 can be obtained directly from the measured values of τ_c and τ_s. Consequently, all other standard critical exponents follow from established scaling relations. For instance, the order-parameter exponent,

$$\beta = (1 - d_f)\nu_1 = \frac{\tau_s - 2}{2 - \tau_c}, \tag{10}$$

Table 2 | The critical exponents τ_c and τ_s for the gap-size distribution $n(G, V, r)$ for $r = r_1$ and $r = r_E$ in various real-world networks

	Biology	Social	Road	Citation	Coauthor	Interaction	Recommendation	Scientific Computing	Gene
τ_c	1.70(1)	1.69(1)	1.77(2)	1.83(2)	1.83(1)	1.63(1)	1.62(2)	1.75(3)	1.70(5)
τ_s	2.76(1)	2.67(3)	2.11(3)	2.82(2)	2.79(3)	2.55(3)	2.56(3)	2.48(2)	2.51(1)
$d_f = \frac{1}{\tau_s - 1}$, $\sigma = 2 - \tau_c$, $\beta = \frac{\tau_s - 2}{2 - \tau_c}$, $\gamma = \frac{3 - \tau_s}{2 - \tau_c}$, $\nu = \frac{\tau_s - 1}{2 - \tau_c}$, $\eta = 2 - \frac{3 - \tau_s}{\tau_s - 1}$									

The estimates of the Fisher exponents are obtained from the least-squares fit to $n(G, V, r)$ (see "Method" for details). Other common critical exponents derived via scaling relations from τ_c and τ_s are presented in the final row.

characterizes the asymptotic scaling behavior of the largest connected component near the percolation transition. This procedure provides a new quantitative perspective for describing network structure and resilience, in which dynamic fragmentation statistics encode universal information traditionally accessible only through idealized FSS analyses. The full set of derived critical exponents for the real-world networks is reported in Table 2.

In Fig. 4(j), we summarize the landscape of universality classes by plotting τ_s versus τ_c. The gray dashed line indicates the theoretical universality class of SF networks with degree exponent $\gamma \in [3, 4)$, for which the relation $\tau_s = \tau_c + 1$ holds via prediction of critical exponents from uncorrelated SF networks[44] (see "Method"). Notably, most real-world networks cluster closer to the universality class of SF networks than to that of high-dimensional lattice systems. This tendency is particularly pronounced for social, citation, and recommendation networks, whose degree distributions are broadly heterogeneous and often exhibit scale-free characteristics. However, although many empirical networks possess degree exponents in the range $\gamma \in (2, 3)$, for example, the recommendation network analyzed above has $\gamma \approx 2.5$, their measured critical exponents (τ_c, τ_s) deviate significantly from the values predicted by idealized model-generated SF networks. This discrepancy highlights that real systems cannot be fully characterized by degree distributions alone. Recent studies have shown that the effective structure of complex networks and clustered core-periphery organization can substantially reshape percolation behavior even when degree statistics appear similar[45,46]. Instead, higher-order structural features, such as meso-scale modularity, tight-knit communities, and hierarchical core-periphery structures, can substantially alter the pathways of connectivity loss, leading real-world networks to cluster into distinct universality classes.

Interestingly, the empirical networks considered here appear to occupy a constrained region of the (τ_c, τ_s) plane. Road networks lie close to the low-dimensional region, consistent with their spatial embedding and relatively narrow degree distribution, whereas many social, citation, and recommendation networks lie closer to the region occupied by heterogeneous SF networks. Moreover, few empirical systems extend substantially beyond the broad envelope traced by SF networks with different degree exponents. This observation suggests that common structural constraints in real-world networks, such as sparsity, degree heterogeneity, clustering, assortativity, spatial embedding, and growth mechanisms, may restrict the accessible region of universality classes. Whether this envelope represents a general constraint on empirical network universality remains an interesting question for future work.

Further, the location of a system in the (τ_c, τ_s) plane has a direct physical interpretation. Since τ_s coincides with the Fisher exponent τ, larger values of τ_s correspond to a narrower critical cluster-size distribution, whereas smaller values indicate broader cluster statistics. By contrast, $\tau_c = 2 - \sigma$, where σ controls the divergence of the characteristic cluster size; larger τ_c, corresponding to smaller σ, indicates stronger fluctuations and more pronounced multiscale organization. This interpretation is consistent with the positions of model systems in Fig. 4(j): low-dimensional lattices exhibit relatively large τ_c and smaller τ_s, reflecting strong fluctuations and broad cluster distributions, whereas high-dimensional and random-graph-like systems display smaller τ_c and larger τ_s, consistent with more mean-field-like behavior. SF networks occupy a distinctive region in which both exponents can be large, suggesting a combination of heterogeneous cluster statistics and strong fluctuation effects. This perspective helps explain why FSS in SF networks can be particularly rich and sensitive to structural details such as the degree exponent and cutoff.

Moreover, the critical exponents extracted from real-world networks are not artifacts of specific modeling assumptions, but instead reflect intrinsic structural properties of the underlying systems. Networks that share similar topological organization exhibit consistent values of (τ_c, τ_s), thereby belonging to the same universality class. This robustness is illustrated in Supplementary Fig. 6, where multiple Facebook network subsets drawn from Ref. 43 are analyzed independently. Despite substantial differences in network size, density, and community composition, the critical exponents obtained from these distinct social systems converge to nearly identical values, demonstrating the stability of universality classification across heterogeneous realizations.

Beyond static network structure, the dynamic scaling framework introduced here further enables characterization of time-evolving systems. We apply the method to temporal journal citation networks[47], in which networks are constructed from citation records over successive decades. As shown in Fig. 5, percolation data derived from networks corresponding to different time intervals collapse onto a single universal scaling curve with high precision. This result indicates that citation networks across time belong to the same universality class, despite continuous growth and structural evolution.

Discussion

In this work, we develop a dynamic framework for percolation on complex networks that reveals previously inaccessible universal features of fragmentation processes. By analyzing the gap-size statistics arising during the growth of the largest connected component, we uncover temporal self-similarity in both the critical and supercritical regimes. This behavior is characterized by two independent Fisher-type exponents, τ_c and τ_s, which can be related to other common critical exponents through the scaling relations $\tau_c = 2 - \sigma$ and $\tau_s = 1 + 1/d_f$, respectively. These exponents form a complete set of descriptors from which the remaining standard critical exponents can be derived through established scaling relations. As a result, the universality class of percolation can be determined for both model-generated and real-world networks, even when only a single system size is available and the critical threshold is unknown. Notably, the present framework builds on the previous largest-gap approach[33], but moves beyond it by shifting the object of analysis from a single extreme-event observable to the full statistical ensemble of growth gaps. While the largest gap provides an effective indicator of the pseudocritical point, the full gap-size distribution captures the statistics of growth events over the percolation trajectory. This distribution-level generalization reveals temporal self-similarity and enables the regime-based gap exponents (τ_c, τ_s) to serve as practical descriptors of universality classes,

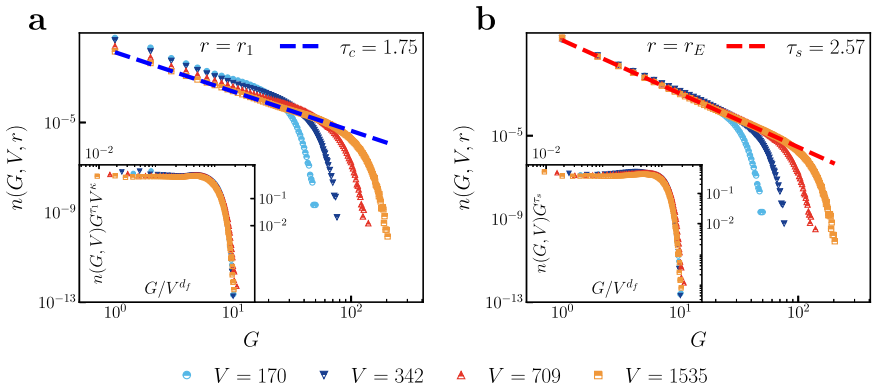


Fig. 5 | Gap-size scaling in temporal journal citation networks. The gap-size distribution $n(G, V)$ is shown as a function of the scaled variables (**a**) r_1 and (**b**) $r_E = V/E$ for bond percolation on the temporal journal citation networks[47]. Different system volumes correspond to networks constructed from citation data across distinct time intervals. The two independent critical exponents are estimated as $(\tau_c, \tau_s) = (1.75(3), 2.57(2))$, while the remaining exponents are derived via the scaling relations given in Eq. (3) and Eq. (9). The inset demonstrates a high-quality data collapse, confirming that percolation on these temporal networks belongs to the same universality class.

especially for empirical networks where conventional finite-size scaling analysis is difficult to implement.

The effectiveness of this dynamic approach originates from three key factors. First, by resolving the full percolation trajectory rather than isolated configurations, our framework continuously characterizes connectivity changes across the entire occupation range, from $r = 0$ to $r = r_E$ (fully occupied). Second, growth gaps of the largest connected component serve as highly sensitive probes of critical behavior, capturing the emergence of macroscopic connectivity. The locations of large gaps accurately identify pseudocritical thresholds, whereas their magnitudes and frequencies encode information about the system's fractal dimension and the width of the critical window. Third, the self-similar scaling structure of the gap-size distribution $n(G, V, r)$ allows critical properties to be extracted from a broad ensemble of intermediate gap events, rather than relying exclusively on extreme fluctuations.

Beyond standard percolation, our framework exhibits considerable generality. As demonstrated in Supplementary Fig. 5, similar dynamic scaling behavior arises in explosive percolation on Erdös-Rényi networks, despite the markedly different nature of the transition[14,39,48–52]. These results suggest that gap-based scaling captures fundamental dynamical features of connectivity transitions that extend beyond classical continuous percolation models. While the present study focuses on single-layer networks with pairwise interactions, the framework can be naturally generalized to more complex interaction structures. Recent studies have shown that higher-order interactions can turn percolation into a genuinely dynamical process[29], while feature-enriched and adaptive networks can substantially reshape critical thresholds and fragmentation pathways[27,28]. Potential extensions therefore include higher-order networks and triadic interactions[29,53] and multilayer or multiplex systems[54–56], where critical phenomena often emerge from the interplay between multiple interaction channels. Recent work on systemic cascades has revealed hybrid universality classes beyond classical expectations[32], abrupt transitions driven by internal random cascading mechanisms in interdependent systems[57], and percolation transitions in non-ideal physical systems such as entangled granular networks[58]. These developments suggest that dynamic scaling may provide a general route for identifying universality classes in complex systems where conventional renormalization or finite-size approaches are difficult to implement.

More broadly, this dynamic scaling perspective provides a useful mathematical bridge between statistical physics and the prediction of real-world catastrophic transitions. Many critical earth and ecological systems exhibit abrupt structural collapses driven by cumulative localized failures, yet they often lack perfect replicas or well-behaved control parameters. Representative examples include ecological fragmentation in coastal and tropical forest systems[2,59], the catastrophic melting of Arctic sea ice[60], and dynamical percolation transitions in urban traffic and climate networks[3,61]. Data-driven dismantling and early-warning analyses, together with recent evidence of nucleation-driven collapse in spatial k-core systems, further emphasize the need for dynamic diagnostics beyond static observables[62,63]. In these highly critical contexts, our gap-based dynamic framework offers a tractable, rigorously grounded diagnostic tool to quantify resilience loss and anticipate systemic reorganization. By decoding the temporal footprint of structural merging, this approach extends the predictive power of statistical mechanics to empirical complex systems.

Dynamic gap scaling offers a unified and scalable framework for diagnosing universality in complex systems. By leveraging temporal information encoded in growth processes, this approach extends universality analysis from idealized models to empirical and evolving networks, opening new avenues for understanding critical transitions in heterogeneous systems.

Methods

Theoretical prediction of percolation critical exponents on the SF networks

For uncorrelated SF networks with degree exponent $\gamma \in [3, 4)$, the standard percolation exponents are[44]

$$\tau = \frac{2\gamma - 3}{\gamma - 2}, \qquad \sigma = \frac{\gamma - 3}{\gamma - 2}. \tag{11}$$

In the present gap-exponent representation, the supercritical exponent satisfies $\tau_s = \tau$, whereas the critical-regime gap exponent satisfies $\tau_c = 2 - \sigma$. Therefore,

$$\tau_c = 2 - \frac{\gamma - 3}{\gamma - 2} = \frac{\gamma - 1}{\gamma - 2}, \tag{12}$$

and

$$\tau_s = \frac{2\gamma - 3}{\gamma - 2} = \tau_c + 1. \tag{13}$$

Thus, the SF reference line in the (τ_c, τ_s) plane follows directly from known SF percolation theory, expressed in the gap-statistics notation used in this work.

Simulation

We simulate percolation using the Newman–Ziff algorithm[22] combined with a union-find data structure, which enables efficient tracking of cluster merging during the dynamic addition of bonds. Bonds are added sequentially, and the size of the largest connected component is recorded at each step of the percolation process.

At each bond-addition step T, we record the unnormalized and normalized growth gap of the largest connected component,

$$G(T) = C(T) - C(T-1), \qquad \Delta(T) = \frac{G(T)}{V}, \tag{14}$$

where $C(T)$ is the size of the largest connected component after T bonds have been occupied and V is the system volume. For the mth-largest gap, its location is defined as $r_m = T_m/E$, where T_m corresponds to the step at which the gap Δ_m occurs and E is the total number of edges. The corresponding largest cluster size is given by $C_m = C(T_m)$. This dynamic percolation process is demonstrated in the Supplementary Movie 1.

In addition, we also record all unnormalized growth gaps of the largest connected component and construct the gap-size distribution $n(G, V, r)$ over the percolation process, which is defined as the gap number density during the bond-adding process with bond fraction from 0 to r with given unnormalized gap size G. Here, we note that the ordered largest-gap analysis in Fig. 2 uses the normalized quantity Δ_m, whereas the gap-size distribution $n(G, V, r)$ is constructed from the unnormalized gap size G. Under this convention, the cutoff of $n(G, V, r)$ scales as $G \sim O(V^{d_f})$.

For simulations on various networks, bonds are stored using a linked-list data structure rather than an adjacency matrix, which substantially reduces memory requirements and allows simulations of large systems. Random-regular and scale-free networks are generated via the configuration model. All real-world networks are sourced from publicly available datasets[43,47]. Each network is treated as unweighted, with self-loops and multiple edges removed during preprocessing. The structural properties of the processed networks are summarized in Supplementary Table S2. For system sizes $V > 10^6$, more than 10^5 independent realizations are generated, while for $V < 10^6$, at least 10^6 realizations are used to ensure statistical convergence.

Data analysis

To extract the critical exponents τ_c and τ_s, we perform a nonlinear fitting via the Levenberg–Marquardt algorithm. For model-generated networks, where multiple system sizes are available, the exponents τ_c and τ_s are estimated through FSS analyses of the total number of gaps $N_G = V\sum_G n(G, V, r)$ at r_1 and the second moment of the gap-size distribution $S_2 = \sum_G G^2 n(G, V, r)$ at r_E, respectively. Systematic uncertainties are assessed by employing multiple fitting forms and comparing the resulting exponent estimates. In contrast, for empirical networks, where only a single system size is typically available, conventional FSS analysis cannot be performed. We therefore estimate τ_c and τ_s directly from the power-law regimes of $n(G, V, r_1)$ and $n(G, V, r_E)$, respectively. The fitting is restricted to the intermediate scaling range, and the uncertainties are estimated by varying the fitting interval.

Details for Fig. 1

The resilience curves shown in Fig. 1a are obtained from Monte Carlo simulations of bond percolation on two-dimensional lattices with system volume $V = 1024^2$. Different curves correspond to distinct lattice geometries, including square, triangular, and hexagonal lattices. For these planar lattices, the exact critical thresholds are known and can be derived from duality and star–triangle relations[64]. For Fig. 1b and Fig. 1c, the normalized size of the largest connected component, denoted as $\tilde{C}$, is calculated using the self-consistent equations of the generating function formalism[8]. In Fig. 1b, the curves correspond to Erdös–Rényi networks with mean degrees $\langle k\rangle$ = 3, 4, and 6, respectively. The associated critical thresholds are given by $q_c = 1 - 1/\langle k\rangle$. For scale-free networks shown in Fig. 1(c), the average degree cannot be prescribed directly. Instead, networks are generated by fixing the minimum degree, while the maximum degree is set to $k_{\max} = 100$ for all realizations. The critical threshold is calculated from $q_c = \frac{\langle k\rangle}{\langle k^2\rangle - \langle k\rangle}$.

Details for Fig. 3

In Fig. 3a, the rescaled size of the largest connected component, $\tilde{C}$, is obtained from a single realization of bond percolation on a two-dimensional square lattice with system volume $V = 128^2$. Figures 3b–d show the corresponding network configurations at bond occupation fractions r = 0.45, 0.5, and 1.0, respectively.

Details for Fig. 5

The temporal networks shown in Fig. 5 are constructed from the Journal Citation Network dataset reported in Ref. 47. Networks of increasing size correspond to citation records aggregated over successive time intervals: 1900–1909, 1919–1928, 1938–1947, and 1952–1961, respectively.

Data availability

The empirical networks used in this work are included in the GitHub repository (https://github.com/hopeless66274/Network_Universality_Class.git)[65] and originate from Refs. 43,47.

Code availability

The Fortran and Python codes used for the analysis are available on GitHub (https://github.com/hopeless66274/Network_Universality_Class.git)[65].

References

1. Gao, J., Barzel, B. & Barabási, A.-L. Universal resilience patterns in complex networks. *Nature* **530**, 307–312 (2016).
2. Scheffer, M., Carpenter, S., Foley, J. A., Folke, C. & Walker, B. Catastrophic shifts in ecosystems. *Nature* **413**, 591–596 (2001).
3. Zeng, G. et al. Switch between critical percolation modes in city traffic dynamics. *Proc. Natl. Acad. Sci. USA* **116**, 23–28 (2019).
4. Xu, Z. & Chopra, S. S. Interconnectedness enhances network resilience of multimodal public transportation systems for safe-to-fail urban mobility. *Nat. Commun.* **14**, 4291 (2023).
5. Dong, G. et al. Resilience of networks with community structure behaves as if under an external field. *Proc. Natl. Acad. Sci. USA* **115**, 6911–6915 (2018).
6. Mittal, K. M., Timme, M. & Schröder, M. Efficient self-organization of informal public transport networks. *Nat. Commun.* **15**, 4910 (2024).
7. Kim, M., Diggans, C. T. & Radicchi, F. Modeling resource consumption in the US air transportation system via minimum-cost percolation. *Nat. Commun.* **16**, 8105 (2025).
8. Newman, M. et al. *Networks* (Oxford University Press, 2018).
9. Liu, X. et al. Network resilience. *Phys. Rep.* **971**, 1–108 (2022).
10. Artime, O. et al. Robustness and resilience of complex networks. *Nat. Rev. Phys.* **6**, 114–131 (2024).
11. Dong, G. et al. Optimal resilience of modular interacting networks. *Proc. Natl. Acad. Sci. USA* **118**, e1922831118 (2021).
12. Folke, C. et al. Resilience: the emergence of a perspective for social–ecological systems analyses. *Glob. Environ. Change* **16**, 253–267 (2006).
13. Cohen, R., Erez, K., ben Avraham, D. & Havlin, S. Resilience of the internet to random breakdowns. *Phys. Rev. Lett.* **85**, 4626–4628 (2000).
14. D'Souza, R. M., Gómez-Gardeñes, J., Nagler, J. & Arenas, A. Explosive phenomena in complex networks. *Adv. Phys.* **68**, 123–223 (2019).

15. Buldyrev, S. V., Parshani, R., Paul, G., Eugene, S. H. & Havlin, S. Catastrophic cascade of failures in interdependent networks. *Nature* **464**, 1025–1028 (2010).
16. Gao, J., Buldyrev, S. V., Stanley, H. E. & Havlin, S. Networks formed from interdependent networks. *Nat. Phys.* **8**, 40–48 (2012).
17. Morone, F. & Makse, H. A. Influence maximization in complex networks through optimal percolation. *Nature* **524**, 65–68 (2015).
18. Saberi, A. A. et al. Recent advances in percolation theory and its applications. *Phys. Rep.* **578**, 1–32 (2015).
19. López, E., Parshani, R., Cohen, R., Carmi, S. & Havlin, S. Limited path percolation in complex networks. *Phys. Rev. Lett.* **99**, 188701 (2007).
20. Stauffer, D. & Aharony, A. *Introduction to Percolation Theory* (Taylor & Francis, 2018).
21. Dorogovtsev, S., Goltsev, A. & Mendes, J. Critical phenomena in complex networks. *Rev. Mod. Phys.* **80**, 1275–1335 (2008).
22. Newman, M. E. J. & Ziff, R. M. Fast Monte Carlo algorithm for site or bond percolation. *Phys. Rev. E* **64**, 016706 (2001).
23. Radicchi, F. et al. Percolation in real interdependent networks. *Nat. Phys.* **11**, 597–602 (2015).
24. Wilson, K. G. et al. The renormalization group and critical phenomena. *Rev. Mod. Phys.* **55**, 583–600 (1983).
25. Pelissetto, A. & Vicari, E. Critical phenomena and renormalization-group theory. *Phys. Rep.* **368**, 549–727 (2002).
26. Cohen, R. & Havlin, S. *Complex Networks: Structure, Robustness and Function*. (Cambridge University Press, 2010).
27. Artime, O. & De Domenico, M. Percolation on feature-enriched interconnected systems. *Nat. Commun.* **12**, 2478 (2021).
28. Rapisardi, G., Kryven, I. & Arenas, A. Percolation in networks with local homeostatic plasticity. *Nat. Commun.* **13**, 122 (2022).
29. Sun, H., Radicchi, F., Kurths, J. & Bianconi, G. The dynamic nature of percolation on networks with triadic interactions. *Nat. Commun.* **14**, 1308 (2023).
30. K. Rizi, A., Michielan, R., Stegehuis, C. & Kivelä, M. Homophily within and across groups. *Nat. Commun.* **16**, 11351 (2025).
31. Millán, A. P. et al. Topology shapes dynamics of higher-order networks. *Nat. Phys.* https://www.nature.com/articles/s41567-024-02757-w (2025).
32. Bonamassa, I., Gross, B., Kertész, J. & Havlin, S. Hybrid universality classes of systemic cascades. *Nat. Commun.* **16**, 1415 (2025).
33. Fan, J. et al. Universal gap scaling in percolation. *Nat. Phys.* **16**, 455–461 (2020).
34. Stanley, H. E. Scaling, universality, and renormalization: three pillars of modern critical phenomena. *Rev. Mod. Phys.* **71**, S358–S366 (1999).
35. Wilson, K. G. Renormalization group and critical phenomena. i. renormalization group and the Kadanoff scaling picture. *Phys. Rev. B* **4**, 3174 (1971).
36. Wilson, K. G. Renormalization group and critical phenomena. ii. phase-space cell analysis of critical behavior. *Phys. Rev. B* **4**, 3184 (1971).
37. Goldenfeld, N. et al. *Lectures on Phase Transitions and the Renormalization Group* (CRC Press, 2018).
38. Gabrielli, A., Garlaschelli, D., Patil, S. P. & Serrano, M. N. Network renormalization. *Nat. Rev. Phys.* **7**, 203–219 (2025).
39. Li, M., Wang, J. & Deng, Y. Explosive percolation obeys standard finite-size scaling in an event-based ensemble. *Phys. Rev. Lett.* **130**, 147101 (2023).
40. Li, M., Fang, S., Fan, J. & Deng, Y. Crossover finite-size scaling theory and its applications in percolation. *arXiv preprint arXiv:2412.06228* (2024).
41. Lu, M., Fang, S., Zhou, Z. & Deng, Y. Interplay of the complete-graph and gaussian fixed-point asymptotics in finite-size scaling of percolation above the upper critical dimension. *Phys. Rev. E* **110**, 044140 (2024).
42. Hu, H., Ziff, R. M. & Deng, Y. No-enclave percolation corresponds to holes in the cluster backbone. *Phys. Rev. Lett.* **117**, 185701 (2016).
43. Rossi, R. A. & Ahmed, N. K. The network data repository with interactive graph analytics and visualization. In *AAAI* https://networkrepository.com. (2015).
44. Cohen, R., ben-Avraham, D. & Havlin, S. Percolation critical exponents in scale-free networks. *Phys. Rev. E* **66**, 036113 (2002).
45. Allard, A. & Hébert-Dufresne, L. Percolation and the effective structure of complex networks. *Phys. Rev. X* **9**, 011023 (2019).
46. Colomer-de Simón, P. & Boguñá, M. Double percolation phase transition in clustered complex networks. *Phys. Rev. X* **4**, 041020 (2014).
47. Hric, D., Kaski, K. & Kivelä, M. Stochastic block model reveals maps of citation patterns and their evolution in time. *J. Informetr.* **12**, 757–783 (2018).
48. Radicchi, F. & Fortunato, S. Explosive percolation in scale-free networks. *Phys. Rev. Lett.* http://link.aps.org/doi/10.1103/PhysRevLett.103.168701. (2009).
49. da Costa, R. A., Dorogovtsev, S. N., Goltsev, A. V. & Mendes, J. F. F. Explosive percolation transition is actually continuous. *Phys. Rev. Lett.* **105**, 255701 (2010).
50. Riordan, O. & Warnke, L. Explosive percolation is continuous. *Science* **333**, 322–324 (2011).
51. Danziger, M. M., Bonamassa, I., Boccaletti, S. & Havlin, S. Dynamic interdependence and competition in multilayer networks. *Nat. Phys.* **15**, 178–185 (2019).
52. Lu, M., Li, M. & Deng, Y. Self-similar dynamics in percolation and sandpile. *Front. Phys.* **21**, 101201– (2026).
53. Brunk, N. E. & Twarock, R. Percolation theory reveals biophysical properties of virus-like particles. *ACS Nano* **15**, 12988–12995 (2021).
54. Bianconi, G. & Radicchi, F. Percolation in real multiplex networks. *Phys. Rev. E* **94**, 060301 (2016).
55. Bianconi, G.*Multilayer Networks: Structure and Function* (Oxford University Press, 2018).
56. de Arruda, G. F., Rodrigues, F. A. & Moreno, Y. Fundamentals of spreading processes in single and multilayer complex networks. *Phys. Rep.* **756**, 1–59 (2018).
57. Gross, B. et al. The random cascading origin of abrupt transitions in interdependent systems. *Nat. Commun.* **16**, 5869 (2025).
58. Kim, S., Wu, D. & Han, Y. Percolation transition in entangled granular networks. *Nat. Commun.* **16**, 11410 (2025).
59. Taubert, F. et al. Global patterns of tropical forest fragmentation. *Nature* **554**, 519–522 (2018).
60. Popović, P., Cael, B. B., Silber, M. & Abbot, D. S. Simple rules govern the patterns of arctic sea ice melt ponds. *Phys. Rev. Lett.* **120**, 148701 (2018).
61. Fan, J., Meng, J., Ashkenazy, Y., Havlin, S. & Schellnhuber, H. J. Climate network percolation reveals the expansion and weakening of the tropical component under global warming. *Proc. Natl. Acad. Sci. USA* **115**, E12128–E12134 (2018).
62. Grassia, M., De Domenico, M. & Mangioni, G. Machine learning dismantling and early-warning signals of disintegration in complex systems. *Nat. Commun.* **12**, 5190 (2021).
63. Xue, L., Gao, S., Gallos, L. K., Havlin, S. & Makse, H. A. Nucleation phenomena and extreme vulnerability of spatial k-core systems. *Nat. Commun.* **15**, 5850 (2024).
64. Baxter, R. J. et al. *Exactly Solved Models In Statistical Mechanics* (Elsevier, 2008).
65. ShengFang_BNU. Shengfangbnu/network_universality_class: Network universality class. https://doi.org/10.5281/zenodo.20731943 (2026).

Acknowledgements

The authors would like to thank Prof. Jürgen Kurths for his valuable discussions.

Author contributions

J.F. designed the research. S.F. and J.M. performed the analysis and prepared the manuscript. S.F., J.M., Q.L., B.C., G.D., C.B., J.N., Y.D., R.L., and J.F. discussed the results and contributed to writing the manuscript.

Fundings

J.F. discloses support for the research of this work from the National Natural Science Foundation of China [T2525011, 42450183, 12275020, 12135003, 42461144209, L2524072], the National Key R&D Program of China [2025YFF0517304], the MEL Visiting Fellowship, and the Fundamental Research Funds for the Central Universities. S.F. discloses support for the research of this work from the National Natural Science Foundation of China [12505036]. J.M. discloses support for the research of this work from the National Natural Science Foundation of China [42575057] and the National Key R&D Program of China [2025YFF0517203]. Q.L., B.C., G.D., C.B., J.N., Y.D., and R.L. declare no relevant funding.

Competing interests

The authors declare no competing interests.

Additional information

Supplementary information The online version contains supplementary material available at (https://doi.org/10.1038/s41467-026-75436-4).

Correspondence and requests for materials should be addressed to Jingfang Fan.

Peer review information : *Nature Communications* thanks anonymous reviewers for their contribution to the peer review of this work. A peer review file is available.

Reprints and permissions information is available at http://www.nature.com/reprints

Publisher's note Springer Nature remains neutral with regard to jurisdictional claims in published maps and institutional affiliations.

Open Access This article is licensed under a Creative Commons Attribution-NonCommercial-NoDerivatives 4.0 International License, which permits any non-commercial use, sharing, distribution and reproduction in any medium or format, as long as you give appropriate credit to the original author(s) and the source, provide a link to the Creative Commons licence, and indicate if you modified the licensed material. You do not have permission under this licence to share adapted material derived from this article or parts of it. The images or other third party material in this article are included in the article's Creative Commons licence, unless indicated otherwise in a credit line to the material. If material is not included in the article's Creative Commons licence and your intended use is not permitted by statutory regulation or exceeds the permitted use, you will need to obtain permission directly from the copyright holder. To view a copy of this licence, visit http://creativecommons.org/licenses/by-nc-nd/4.0/.

© The Author(s) 2026